Physical origin of thickness-controlled sequential phase formation during reactive diffusion: Atomistic modeling

A. Portavoce[1,*] and G. Tréglia[2]
[1]*IM2NP, Faculté des Sciences de Saint-Jérôme, CNRS, case 142, 13397 Marseille, France*
[2]*CINAM, Campus de Luminy, CNRS, case 913, 13288 Marseille, France*
(Received 24 March 2010; revised manuscript received 10 September 2010; published 19 November 2010)

Experimental studies of reactive diffusion during annealing of a film deposited on a substrate reveal that the phase formation proceeds either simultaneously or sequentially depending on the film thickness and that its time dependence exhibits a linear-to-parabolic time-dependence transition. This surprising behavior is investigated here theoretically at the atomistic scale via kinetic Monte Carlo simulations based on an Ising energetic model that preserves the main thermodynamic properties of the model system under study, namely, a *B* substrate with an fcc structure on which a thicker or thinner *A* film is deposited and annealed at a given temperature. We show that the phase growth linear time dependence is related neither to an interface effect nor to diffusion asymmetry but results from the first stage of phase formation in a local composition close to the phase stoichiometry, whereas the following parabolic time dependence is due to the need for atom transport before phase nucleation. In addition, the thickness-controlled sequential phase formation is attributed to the existence of an asymmetric interdiffusion profile that results, even in the case of symmetric diffusion kinetics, from the respective finite and semi-infinite nature of the film and of the substrate.

DOI: 10.1103/PhysRevB.82.205431 PACS number(s): 64.60.Bd, 64.75.Jk, 64.75.Gh, 68.35.Rh

I. INTRODUCTION

Solid-state reactive diffusion is a complex phenomenon involving atom diffusion and phase transformation.[1–3] It plays a major role in many industrial processes (metallurgy,[4–6] microelectronics,[7]…) in which case it can be either damaging or on the contrary advantageously used to produce highly elaborated materials or structures. Although the first studies of reactive diffusion were performed in the metallurgy field at the microscopic scale, a strong need is now felt for a more detailed understanding of its mechanisms at the nanometer scale with the development of new processes that allow for the production of a large variety of nanostructures. At the same time, the macroscopic concepts (such as atom diffusion, phase nucleation, and interfacial reaction), which entered the continuum models and linear equations[8–11] generally used, for example, in systems such as silicides or germanides, have to be revisited at the atomic scale. It has been experimentally observed, as far as interfacial reaction is concerned, that the volume of a new phase can grow according to a law proportional to time during a first stage, and then to the time square root during a second stage.[1] Since kinetics is generally driven by the slowest phenomenon, these observations were interpreted by considering that these two regimes are controlled by two different mechanisms that occur simultaneously during reactive diffusion but that are of different importances at the beginning and at the end of the process (or at different temperatures).[7] In this framework, the first regime is usually attributed to interfacial-reaction kinetics since the thickness of the new phase located between the reactant sources is sufficiently thin to neglect the reactant diffusion kinetic through it. In contrast, as the time square-root behavior is characteristic of the diffusion process, the second regime is usually attributed to atom diffusion kinetics, the reactant diffusion in the new phase becoming now the main limiting process due to the increase in the growing phase thickness. Nevertheless, such a macroscopic interpretation is not so straightforward at the atomic scale if one considers nanoscale effects. In particular, the linear dependence of the growth can be interpreted in many different ways; a modification of the usual square-root law in the case of nanoscale diffusion,[12–15] the beginning of phase nucleation,[16] atom rearrangement processes at the interface to build the growing phase (similar to crystallization),[17–19] the permeability of the interface,[20] or finally important diffusion kinetic differences between the reactants.[21]

Such dimensional effects on the reactive diffusion process have been observed for several systems from intermetallic couples such as Al-Au (Refs. 5 and 6) to silicide formation.[7,9] The reaction between 2-μm-thick pure layers of two different elements (binary system) generally leads to the simultaneous formation of all the phases present in their phase diagram (at a given temperature).[5] On the contrary, if the thickness of at least one of the layers is about tens of nanometer, the formation of the phases can be sequential and some of them can be missing.[6] Despite that this nanometric effect has been experimentally studied for years, its origin is still under discussion.[2,3,22] If several minima (several compounds) exist in a binary system, thermodynamic equilibrium arguments based on the minimization of the enthalpy fail to explain the sequential phase formation and to predict which phases will be missing and which will be the first phase to appear as the starting point of the phase sequence.[1]

Consequently, kinetic arguments have been proposed to explain the experimental observations. However, it has been shown that the missing phase phenomenon cannot be explained from arguments based only on diffusion-controlled phase formation since in that case, the layer growth velocity is infinite for ultrathin layers (no layer can shrink).[23] Therefore, the generally accepted model to qualitatively explain the sequential phase formation and the missing phase phe-

nomenon considers both the diffusion and reaction kinetics.[8–11] Let us point out however that these models do not account for the phase nucleation process but rather start from an initial state in which some phases coexist between the two pure layers. Then, the volume growth/reduction competition between all the phases is simulated by considering that diffusion-controlled and interfacial-reaction-controlled processes are simultaneously operative, which indeed reproduces the linear to parabolic time-dependence transition of the phase volume. In contrast to Kidson's analysis,[23] it is found that depending on the diffusion flux ratios of the reacting elements in the different phases (which depend on the diffusion and interfacial-reaction coefficients) some phases may shrink while others should grow, leading to missing phases. Furthermore, for a given phase, a critical thickness may exist below which only this phase can grow, explaining the possible occurrence of sequential phase formation. Actually, if the thickness of the layer deposited on the substrate is smaller than this critical thickness, a single phase will grow up to the total consumption of the initial film, after which a second single phase can start growing if the thickness of the first phase is also lower than a corresponding critical thickness.

The goal of the present work is to further investigate reactive diffusion at the atomic scale, using a model able to simultaneously account for the equilibrium driving forces, the diffusion and reaction kinetics, and the nucleation process in order to better understand the atomistic meaning of the reaction coefficient and to identify the origin of sequential phase formation. To this aim we use a kinetic Monte Carlo (KMC) technique to simulate the kinetic evolution of a model binary A/B system built on a rigid fcc lattice for two A and B species which present a symmetrical phase diagram (symmetrical phase formation enthalpy and solubility limit around the 50% composition), in absence of any diffusion asymmetry (constant diffusion barrier). Our simulations indeed lead to the two experimental transitions (from a linear-to-parabolic time-dependence transition of phase growth on the one hand, and from simultaneous-to-sequential phase formation on the other hand) while clarifying their physical origin. Thus, the linear time dependence of phase growth is due to the first stage of atom ordering, which may be interpreted as a nucleation process, and is related neither to an interface effect nor to diffusion asymmetry. Then, depending on the initial thickness of the deposited film, three regimes are observed: (i) phase coexistence for thick layers, (ii) quasisimultaneous phase formation followed by sequential phase dissolution for intermediate thicknesses, and (iii) sequential phase formation for the thinnest layers. In this last case, the sequential phase formation results from the existence, even for symmetric diffusion kinetics, of an asymmetric interdiffusion profile due to the finite nature of the deposited layer and the semi-infinite nature of the substrate.

II. KINETIC TIGHT-BINDING ISING MODEL

The goal of this study is not to simulate the reactive diffusion in a given A/B binary system but more generally to identify the atomic mechanisms that drive reactive diffusion transformations and to correlate them with the experimental macroscopic observations. To this aim both the energetic model describing the interactions between the atoms and the kinetic Monte Carlo simulation have to be simple enough to allow us to use systematic calculations.

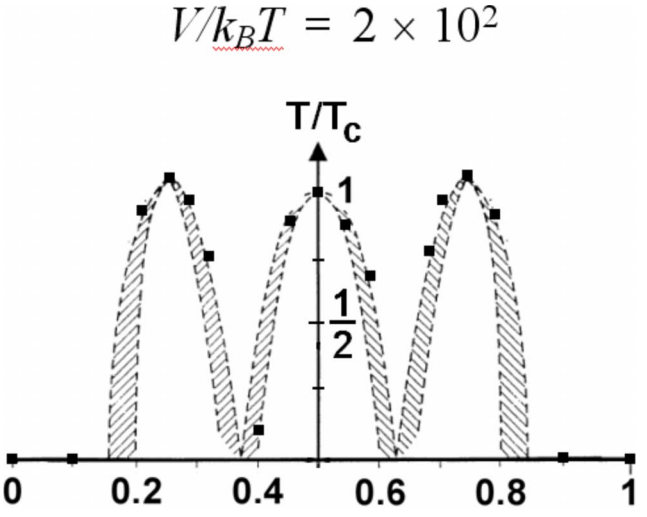

FIG. 1. (Color online) Phase diagram of an ordered binary nonregular fcc solid solution. Compositions around 25% and 75% correspond to $L1_2$ phases while compositions around 50% correspond to the $L1_0$ phase. Lines are from Ref. 27, squares correspond to our calculations, we found $T_c=3673$ K with $V/k_BT=2\times10^2$.

As the basis of the model has already been described in several papers,[24,25] here we only give a brief survey of the energetic model used in our kinetic model. It is based on an effective Ising Hamiltonian derived from electronic-structure calculations tight binding Ising model (TBIM) for surface segregation problems.[26] More precisely, the total energy of the binary system is decomposed in pairwise interactions between first neighbors V_{AA}, V_{BB}, and V_{AB}, under the constraint that these interactions preserve both the difference in surface energies between the A and B elements [$\Delta\tau=Z'(V_{AA}-V_{BB})$, Z' being the number of broken bonds at the surface], and the essential thermodynamics of the A_cB_{1-c} alloy that is driven by the value of the single parameter $V=\frac{1}{2}(V_{AA}+V_{BB}-2V_{AB})$, the value of which gives its mixing energy and therefore its tendency to phase separation ($V<0$) or ordering ($V>0$). The purpose of our study being to understand the general trend of reactive diffusion, we are interested here in systems that display a strong tendency to bulk ordering (large positive value of V), and then a bulk phase diagram presenting several (at least two) ordered compounds in order to observe and study the thickness-controlled simultaneous-to-sequential phase formation transition. As shown in Fig. 1, for interactions limited to first neighbors, the fcc lattice has the advantage of offering the stabilization of three ordered phases as a function of concentration, centered around the 25% ($L1_2$ phase), 50% ($L1_0$ phase), and 75% ($L1_2$ phase) concentrations (C). Such binary systems also exhibit symmetric phase enthalpies and symmetric solubilities around the 50% solution composition. Finally, in order to follow as closely as possible the phase formation sequences, V and T (temperature) will be chosen such that the ratio $V/k_BT=2\times10^2$ corresponding to a

temperature ratio T/T_c of $\sim 3\times 10^{-3}$, with k_B the Boltzmann constant and T_c the $L1_0$ order/disorder critical temperature. In this case, one can see in Fig. 1 that the A-rich $L1_2$, $L1_0$ and B-rich $L1_2$ are, respectively, found for $0.64 \leq C_A \leq 0.84$, $0.38 \leq C_A \leq 0.64$ and $0.16 \leq C_A \leq 0.38$. Furthermore, in order to neglect the surface segregation effect and to study a symmetric binary system, we will limit our study to the case $V_{AA}=V_{BB}$. In this case, we have checked that the nature of the segregating element only depends on bulk concentration in our system: segregation of the majority element in the solid solution (e.g., $C=0.1$ in Fig. 1), and most stable termination of the bulk ordered phase ($L1_2$ or $L1_0$) for ordered compounds (e.g., $C=0.25$ in Fig. 1).

In order to follow the dissolution of the deposited film A/B, the reactive diffusion time scale (atomic transport and ordering) imposes the use of KMC simulations on rigid atomic lattice (here fcc as previously mentioned). KMC allows the exact solution of the reactive diffusion phenomenon to be obtained, taking into account the thermodynamic equilibrium driving forces, the atomic transport and ordering kinetics, as well as nucleation, surface segregation, the possible formation of nonordered solid solutions, and phase mixing. Its realization is performed using the standard Metropolis algorithm[28] rejecting and accepting configurations according to the internal energy given by the Ising model given above. Then, by allowing exchanges between first-neighboring atoms only, as described in detail in previous papers by Roussel *et al.*,[29–31] we can simulate an effective diffusion process in which the atomistic diffusion elementary mechanisms have been replaced by effective exchanges on the atomic lattice, and describe the thermodynamic evolution of the system. Note that in this framework, we do not introduce any asymmetry of the bulk diffusion coefficient. The diffusion barrier is then nothing other than a scaling factor, so we did not specify its value. Instead, since the relative time (t) is only needed for our investigation, we will use one Monte Carlo cycle (MCC) as the time unit, which corresponds to a sequence in which every atom of the box is offered to change its position once. For dissolution of a thick deposited layer, the initial condition mimics the experimental starting condition: a given number of full layers of A atoms (minority) are located over a substrate of B atoms (majority). We perform simulations in a box of $(l\times l\times m)$ fcc unit cells with periodic boundary conditions in the direction parallel to the surface. In the direction perpendicular to the surface, a free (001) surface is considered on one side while on the opposite side each atom arriving in the bottom plane is removed to simulate a $C=0$ boundary condition. The choice of the m value is then crucial since, if for instance the penetration length of A atoms is greater than m, this boundary condition will accelerate the kinetics. To avoid any drawbacks due to the finite size of the box in dissolution kinetics, one uses systems such as $l=16$ and $m=319$, which leads to atomic boxes of $\sim$210 000 atoms. The kinetic evolutions shown in the figures have been obtained by averaging, for every given MCC, the results of 30 independent simulations performed with same settings (system size, temperature,…), and same initial conditions. If otherwise, simulations settings are stated in the text or in the figure's caption. Single simulations using time averages upon 100 or 1000 atomic Monte Carlo events gave similar results ($\sim$210 000 events for one MCC).

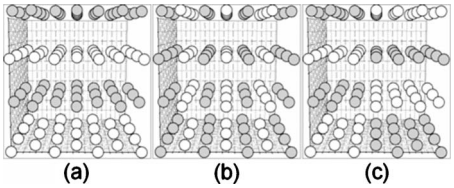

FIG. 2. $L1_0$ ordered cells of stoichiometry $C=0.5$, containing 100 atoms: (a) cell ordered along the [001] direction, (b) cell ordered in the [100] direction, and (c) cell containing two domains ordered along the [001] direction, shifted by one atomic plane.

III. DATA ANALYSIS

The study of three-dimensional (3D) phase formation at the atomic scale is not easy since the detection of the ordered phases is complicated by the possible formation of 3D ordered domains with different variants, and different compositions in the case of nonstoichiometric compounds. As an illustration, Fig. 2 presents three $L1_0$ ordered cells containing 100 atoms and corresponding to the same stoichiometry $C=0.5$. In Fig. 2(a) the cell is ordered along the [001] direction while in Fig. 2(b) the cell is ordered along the [100] direction according to another variant, and in Fig. 2(c) the cell contains two domains ordered along the [001] direction [same variant as in Fig. 2(a)] but shifted by one atomic plane. Consequently, phase detection and identification cannot be based simply on one-dimensional (1D) profile concentration. For example, the $L1_0$ order can be identified in the concentration profile along the [001] direction as an alternate stacking of pure A and B layers in Fig. 2(a) but not in Figs. 2(b) and 2(c) since the composition of all the (001) planes is 50%. It is then necessary to develop an algorithm that would allow us to identify the presence of a given ordered phase no matter what the situation is.

To this aim, we consider as the elementary domain of a given ordered phase the 13-atom cuboctahedron built from one atom and its first coordination shell on the fcc lattice. Using this criterion, it is possible to calculate the proportion of atoms on the lattice that are ordered following the A-rich $L1_2$ structure ($A_{0.75}B_{0.25}$ compound), the $L1_0$ structure ($A_{0.5}B_{0.5}$ compound), or the B-rich $L1_2$ structure ($A_{0.25}B_{0.75}$ compound) in the three spatial directions. This way, we then have access to the evolution of the three phase volume fractions (F_0) versus time. It should be mentioned that this criterion does not apply to the atoms in the surface plane ($P=1$) since the calculation requires 12 neighbors. One can also note that in our case, the fcc lattice being rigid (not relaxed), the three phases are cubic. Our algorithm relies on the spatial distribution of atoms in this 13-atom elementary domain, considering phase ordering in the x, y, and z directions only. This independent 13-atom cell contains three planes in each x,y,z direction, the first plane containing $4\times 1/4$ atoms (one atom is shared by four cells), the second containing $4\times 1/4+1$ atoms, and the third $4\times 1/4$ atoms. In each direction i (=x, y, or z), the atomic fraction of A atoms in each of

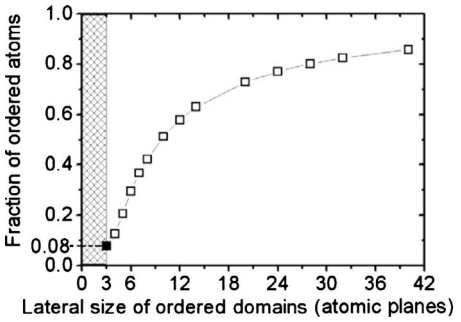

FIG. 3. Variation in the volume fraction of ordered atoms versus domain lateral size, if the layer bulk is made of same cubic domains ordered in different directions.

the three planes (C_1^i, C_2^i, and C_3^i) can be calculated and summed ($\Sigma_i = C_1^i + C_2^i + C_3^i$). Thus, it can be shown that each possible order (or phase) oriented along x, y, or z corresponds to different Σ_x, Σ_y, and Σ_z combinations, which are also different from the disorder case. This simple algorithm allows the differentiation of each phase from disorder. For example, for the $L1_0$ order the concentration of A atoms over three sequential atomic planes varies as 1/0/1 or 0/1/0 (Fig. 2). The cell order corresponds to the $L1_0$ phase, only if $\Sigma_z = 1$ and $\Sigma_x + \Sigma_y = 3$ (0/1/0 along z), or $\Sigma_z = 2$ and $\Sigma_x + \Sigma_y = 3$ (1/0/1 along z), or $\Sigma_z = 1.5$ and $\Sigma_x + \Sigma_y = 2.5$ (0/1/0 along x or y) or 3.5 (1/0/1 along x or y). Obviously, if the total volume is ordered with domains of the same structure but with different orientations, the total fraction of ordered atoms will not be equal to 1 since the domain boundaries will not be strictly ordered according to the considered structure. In order to quantify the critical value of F_0 beyond which one can consider that the volume of the sample is made only of the corresponding phase, we plot in Fig. 3 the variation in the volume fraction of ordered atoms with the lateral size of ordered cubic domains if the total volume is filled with these domains. A cubic domain with a lateral size of three atomic planes ($3P$ domain) corresponds to the smallest possible domain, made of one atom and its 12 first neighbors. It is worth noting that if the totality of the sample is ordered but made of $3P$ domains, the volume can be considered as uniformly made of the same phase although the ordered atom fraction is only ~ 0.08 because of domain boundaries. Consequently, if we measure $F_0 \geq 0.08$ for a given phase, the volume of the sample can be made of this phase only. On the contrary, it cannot contain this only phase if $F_0 < 0.08$ (filled area in Fig. 3), which is, for example, the case of isolated $3P$ domains in a nonordered A-B solid solution (beginning of the nucleation process).

In order to follow the phase thickness variations in the [001] direction, we calculate in each {001} plane the three fractions F_0 corresponding to the three possible structures: A-rich $L1_2$, $L1_0$, and B-rich $L1_2$. This is illustrated in Fig. 4, in the case of the dissolution of a 50-monolayer (ML)-thick A layer on a B substrate at two different annealing times: $t = 140$ MCC [Fig. 4(a)] and $t = 680$ MCC [Fig. 4(b)]. These results were not averaged in order to compare the volume fractions to the one-dimensional (concentration profile) and the three-dimensional (atoms on the lattice) atom distribu-

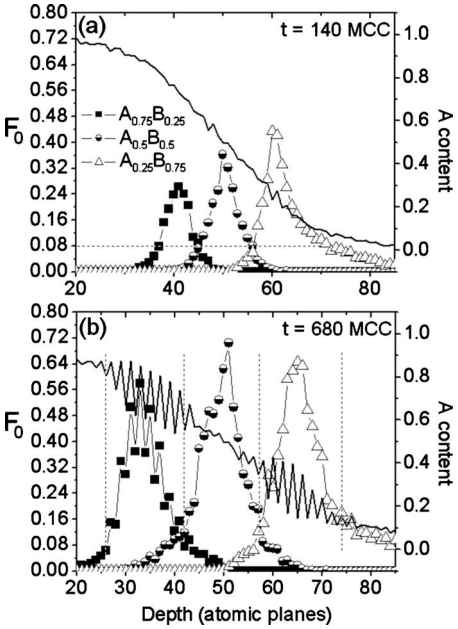

FIG. 4. Volume fraction F_0 (left axis) of the three ordered phases A-rich $L1_2$ (solid squares), $L1_0$ (semisolid circles) and B-rich $L1_2$ (open triangles), and concentration profile of A atoms (solid line, right axis) versus depth (atomic planes, bottom axis) in the case of the dissolution of a 50-ML-thick A layer on a B substrate: instantaneous results (a) $t = 140$ MCC and (b) $t = 680$ MCC.

tions. This figure allows us to correlate the concentration profile of A atoms (solid line, right axis) to the ordered fractions (left axis) of the three structures A-rich $L1_2$ (solid squares), $L1_0$ (semisolid circles), and B-rich $L1_2$ (open triangles) as a function of the incorporation depth (atomic planes, bottom axis).

For short annealing times, the 3D atom distribution shows that the phases are constituted of small domains ordered in different spatial directions so that the phases cannot be detected in the 1D concentration profile. Thus, after 140 MCC, as can be seen in Fig. 4(a), the concentration profile C_A varies quite smoothly from 1 to 0, with a shape that is rather symmetric around 0.5. However, the ordered fractions of the three structures versus depth show that the three phases coexist at the time of the dissolution, the A-rich $L1_2$ phase being located between the atomic planes 36 and 45, the $L1_0$ phase between the planes 45 and 56, and the B-rich $L1_2$ phase between the planes 56 and 71. The comparison between the concentration domains of existence of the three bulk ordered phases at this temperature displayed in Fig. 1 and those of the finite compounds formed during dissolution [solid line in Fig. 4(a)], shows that they are fully consistent since the latter are found, respectively, for $0.65 \leq C_A \leq 0.83$ (A-rich $L1_2$), $0.40 \leq C_A \leq 0.65$ ($L1_0$), and $0.16 \leq C_A \leq 0.40$ (B-rich $L1_2$).

For longer annealing times, the domains grow bigger and tend to get ordered in the same direction (usual energy minimization) so that the different phases can be more easily detected in the 1D concentration profile, particularly if the atom ordering direction (normal to the atomic planes of sequential compositions) is perpendicular to the [001] crystal

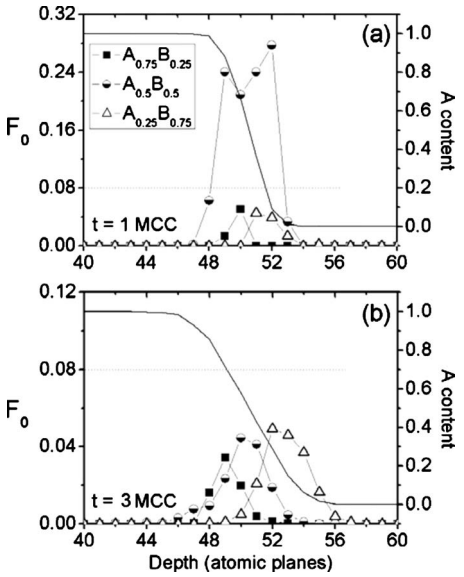

FIG. 5. Volume fraction F_0 (left axis) of the three ordered phases A-rich $L1_2$ (solid squares), $L1_0$ (semisolid circles) and B-rich $L1_2$ (open triangles), and concentration profile of A atoms (solid line, right axis) versus depth (atomic planes, bottom axis) in the case of the dissolution of a 50-ML-thick A layer on a B substrate: (a) $t=1$ MCC and (b) $t=3$ MCC.

direction [Fig. 2(a)]. Thus, Fig. 4(b) shows that the lateral domain size has increased from ~7 atomic layers ($F_0 \sim 0.35$) at $t=140$ MCC, up to ~15 atomic layers ($F_0 \sim 0.65$) at $t=680$ MCC. Furthermore, the A-concentration profile in the latter case now reveals the alternate stacking of A-rich and B-rich layers at two different depths. The region that is the closest to the surface (between the atomic planes 27 and 45) corresponds to the A-rich $L1_2$ structure (which in the perfectly ordered compound leads to planes alternating between $C_A=1$ and $C_A=0.5$) that tends to order in the direction perpendicular to the surface, whereas the deeper region (between the atomic planes 57 and 75) corresponds to the B-rich $L1_2$ structure (which in the perfectly ordered compound leads to planes alternating between $C_A=0.5$ and $C_A=0$) that also tends to order along the [001] crystal direction. Between these two regions (atomic planes 45–57) the A concentration profile is smoother, which does not mean that this region is disordered but which corresponds, according to Fig. 4(b), to the $L1_0$ structure ordered along a direction parallel to the surface [in which case $C_A=0.5$ in all the atomic planes for the stoichiometric compound, Fig. 2(b)]. It is worth noting that the regions delimiting the three compound layers on the concentration profile are in good agreement with the ordered fractions for each of the compounds.

IV. PHASE GROWTH TIME DEPENDENCE

Let us now analyze more precisely the time dependence of the dissolution of the previous 50 ML of A into the B substrate. To this aim, we present in Fig. 5 the very first stages of A/B interdiffusion, beginning with the first MCC [Fig. 5(a)]. At this stage, the concentration profile is found to be symmetric with $0 \leq C_A \leq 1$ and, according to our criterion

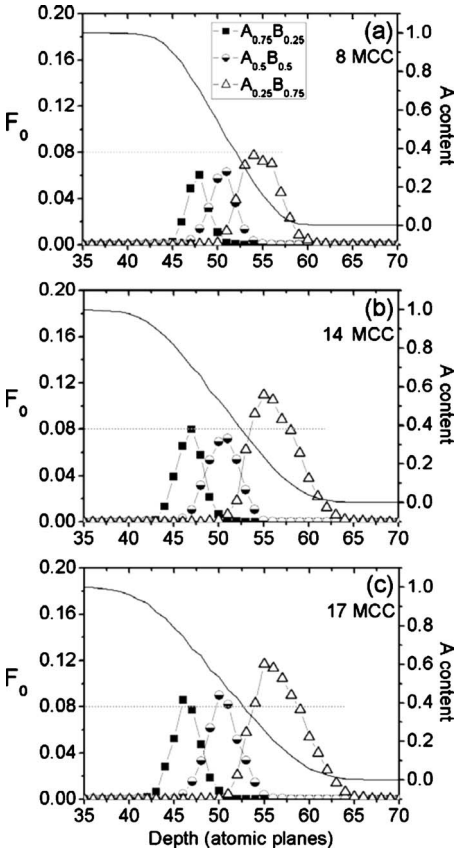

FIG. 6. Volume fraction F_0 (left axis) of the three ordered phases A-rich $L1_2$ (solid squares), $L1_0$ (semisolid circles) and B-rich $L1_2$ (open triangles), and concentration profile of A atoms (solid line, right axis) versus depth (atomic planes, bottom axis) in the case of the dissolution of a 50-ML-thick A layer on a B substrate: (a) $t=8$ MCC, (b) $t=17$ MCC, and (c) $t=20$ MCC.

for compound formation ($F_0 > 0.08$), the single phase that appears is $L1_0$, which already extends upon four layers around the initial AB interface. The lifetime of this compound is very short since it disappears after 3 MCC [see Fig. 5(b)] to the benefit of a few nuclei ($3P$ domains in C gradient, $0 < F_0 < 0.08$) of the three compounds $A_{0.75}B_{0.25}$, $A_{0.5}B_{0.5}$, and $A_{0.25}B_{0.75}$, which coexist along an interfacial concentration that decreases due to A-B interdiffusion following a Fickian[32–34] behavior until the initial phase formation process detailed in Fig. 6. As can be seen from the time sequence presented in this figure, the three phases appear sequentially, with a very short time step of about 5 MCC in average. Thus, after 8 MCC, a first B-rich $L1_2$ compound forms around $C_A \sim 0.25$ while the two other compounds still exist only as isolated nucleuses [Fig. 6(a)]. Then, after 14 MCC, the other $L1_2$ phase (A rich) appears at $C_A \sim 0.75$ and coexists with the previous one [Fig. 6(b)]. Finally, at $t=17$ MCC, the $L1_0$ phase (at $C_A \sim 0.5$) joins the other two in such a way that at the end, the three bulk compounds are found to coexist [Fig. 6(c)]. Taking advantage of the initial coexistence of the three nuclei in the concentration gradient and of the short time required to reach the coexistence of sufficiently thick ordered compounds, one can reasonably consider that the formation of the three phases is quasisimulta-

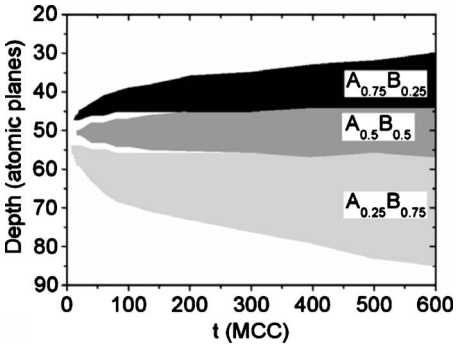

FIG. 7. Depth location of the three phases $A_{0.75}B_{0.25}$, $A_{0.5}B_{0.5}$, and $A_{0.25}B_{0.75}$, from the atomic plane 20 (subsurface plane) to the plane 90 versus time (t), in the case of the dissolution of a 50-ML-thick A layer on a B substrate.

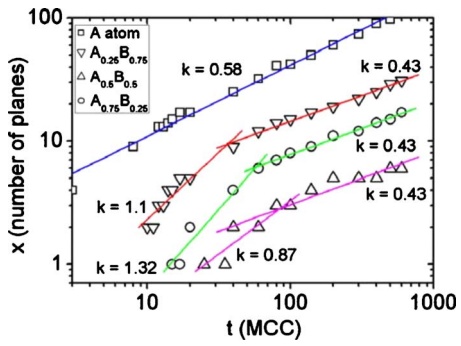

FIG. 8. (Color online) Logarithm of the displacement (x) of A atoms (squares) and of the compound interfaces (down triangles, up triangles, and circles for $A_{0.25}B_{0.75}$, $A_{0.5}B_{0.5}$, and $A_{0.75}B_{0.25}$, respectively) versus the logarithm of time (t), in the case of the dissolution of a 50-ML-thick A layer on a B substrate.

neous. During this process, the concentration gradient stays almost symmetric and covers the entire concentration range from $C_A=1$ ($C_B=0$) to $C_A=0$ ($C_B=1$). The formation of the two $L1_2$ structures before the $L1_0$ one can be understood from simple equilibrium arguments in terms of a lower stability of the latter in the bulk, which can be deduced from their relative order/disorder critical temperatures (see Fig. 1). This effect can be enhanced by kinetic reasons since the atom diffusion flux is proportional to the mobility and to the concentration gradient. As the mobility is constant in our case, this flux is higher in regions of stronger concentration gradient, i.e., as can be seen in Figs. 5 and 6 around the 50% composition, meaning that the stabilization of the $L1_0$ phase could be more difficult than that of the $L1_2$ phases in the regions corresponding to their local composition (lower concentration gradient, lower diffusion flux). Then, once a full layer of each of the three compounds has formed, they all continue to grow simultaneously and independently in the concentration gradient up to ~100 MCC, as illustrated in Fig. 7. From that moment on, the three compounds are in contact with each other, so that the $A_{0.75}B_{0.25}$ and $A_{0.25}B_{0.75}$ films can only grow if B, or, respectively, A, atoms diffuse through the three compound layers. It is worth noting that the sequence described above is representative of all the calculations we performed and that it has been observed for both the A-film-on-B-substrate (A/B) and the B-film-on-A-substrate (B/A) systems, as expected from the symmetric character of our A-B binary system.

In order to more quantitatively determine the growth process of a given phase, we chose to follow the variation in its interfaces over time. Interface mobilities versus time of each of the three ordered compounds and also of individual atoms are shown in Fig. 8, in the case of the previous system (50 ML A/B), x is the interface displacement and k a constant coefficient. For the dilute atom case, x was chosen to be the depth variation with time of the deepest layer atom in the substrate. The same dependence is obviously found in the reversed case B/A due to the symmetry of our A-B system. Let us note that if growth was simply controlled by either reaction or diffusion, the simple law $x \propto t^k$, should be obeyed with $k=1$ in the former case and $k=0.5$ in the latter (Fickian diffusion). As can be seen in this figure, the mobility of individual atoms is found to follow a single behavior versus time during the whole phase growth process with k values close to 0.5 ($k \sim 0.58$), in agreement with the usual Fickian diffusion (constant diffusion barrier in the model). The case of the compound interface displacement is significantly different, with in particular a time-dependence transition from k values close to 1 in a first regime to k values close to 0.5 in a second regime (Fig. 8), in agreement with experimental observations.[1,7,9,11] As mentioned in the introduction, such a behavior is usually explained by an interfacial-reaction-controlled growth in the first regime due to the small thickness of the phases, followed by a diffusion-controlled regime induced by the thickening of the compounds. It should be noted that such an interpretation obviously implies the existence of interfaces and of long-distance atomic transport.

In order to interpret the results of our simulations, and in particular to separate what in the observed behavior is due to the finite character of the system under study, we have also simulated in the same way the kinetics of formation of a single ordered phase in the bulk starting from solid solutions with averaged concentrations corresponding to the three compound compositions ($C_A=0.75$, 0.5, and 0.25). Indeed, as opposed to the previous A/B case, here we do not expect any compound interfaces nor any atom diffusion since, before phase formation, the composition is the same throughout the random solution, which corresponds to the existence of a single stable phase only. The corresponding variations in the $L1_0$ and $L1_2$ phase volume fractions F_0 versus time during this process are shown in Fig. 9(a). In this case, F_0 is not averaged over several simulation runs as we need to compare it with the instantaneous 3D atomic distribution [Fig. 9(b)]. Phase formation exhibits three stages. During the first stage (until $t \sim 33$ MCC), the phase volume fraction increases linearly with time ($k \sim 1$). During the second stage (from 33 to 148 MCC), the volume fraction exhibits almost a square-root dependence with time ($k \sim 0.5$). Finally, in the last stage, F_0 varies slowly toward a constant value. The first two stages are similar to what is observed during reactive diffusion, despite that no long-range concentration gradient and no interfaces are involved in the phase formation. Figure 9(b) presents four successive planes from the solid solution bulk at three different simulation times (15, 120, and 2000 MCC) corresponding to the three volume fractions noted by the

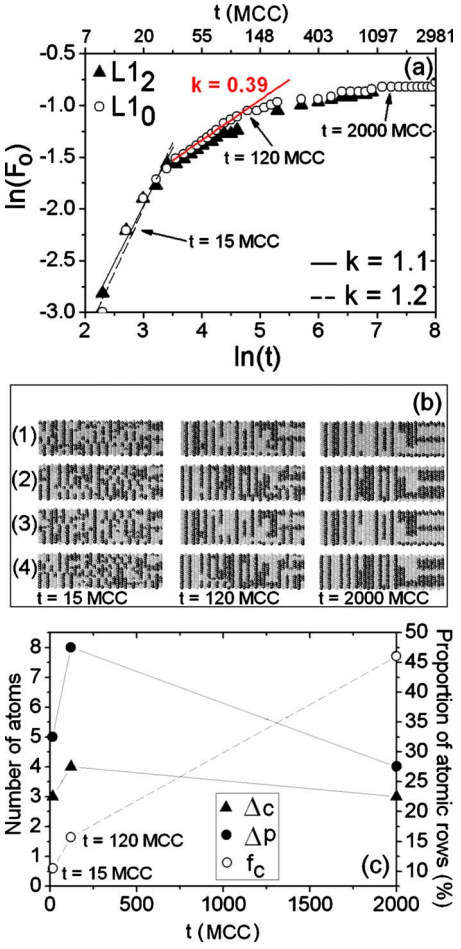

FIG. 9. (Color online) Bulk single phase formation from solid solution of averaged concentration corresponding to the phase stoichiometry: (a) instantaneous variation in the $L1_0$ (open circles) and $L1_2$ (solid triangles) phase volume fraction F_0 versus time, (b) four successive planes from the solid solution bulk at three different times (15, 120, and 2000 MCC) corresponding to the three volume fractions noted by an arrow in the plot of the $L1_0$ phase formation in (a), and (c) average number of atomic exchanges (left axis) between neighbor atomic rows (Δc) and between neighbor atomic planes (Δp), and proportion (right axis) of unchanged atomic rows (f_c) versus time, in the case of the $L1_0$ phase formation presented in (a).

arrows in the plot of the $L1_0$ phase formation in Fig. 9(a). At 15 MCC (linear time-dependence growth) the atom ordering is still weak: some domains start to be visible [alternation of pure *A* /pure *B* regions in the successive planes (1), (2), (3), and (4)] but they are small and have a lot of "defects." The $L1_0$ ordering is more easily observed after 120 MCC, and the domains observed at 120 MCC became bigger at $t=2000$ MCC. Figure 9(c) presents, for the same three considered times (15, 120, and 2000 MCC), the average number of atomic changes between neighboring atomic rows in the [100] direction (Δc) and between neighboring (001) atomic planes (Δp), as well as the proportion of unchanged atomic rows in the [100] direction (f_c). The statistics consider only effective ordering changes, and have been made over same ten consecutive bulk planes, between the considered times. In the linear time-dependence regime, 90% of the atomic rows experience a composition change ($f_c \sim 10\%$), with $\Delta c \sim 3$ and $\Delta p \sim 5$. In the second regime ($k \sim 0.5$), the proportion of modified atomic rows slightly decreases (but remains significant $\sim 83\%$) while the average number of atomic exchanges increases ($\Delta c \sim 4$ and $\Delta p \sim 8$). Finally, in the last regime, both atomic row ordering and atomic exchanges are decreasing: 46% of atomic rows are unchanged, with $\Delta c \sim 3$ and $\Delta p \sim 4$. Consequently, the linear growth time dependence appears to be related to the beginning of the ordering process, which can be considered to be the domain nucleation process. The degree of reordering is high ($f_c \sim 10\%$), and we observe the formation of domains with a high level of ordering defects, relatively low atomic exchanges (about the same as when the domains are formed in the last regime) that together with $k \sim 1$ mean that, at this ordering stage, only atoms from a close vicinity are used to form the domain nucleus (no long-distance atomic transport). Furthermore, in this regime, few atom displacements (single jumps) allow a significant decrease in the system's total energy. The second regime corresponds to both the improvement of in-domain ordering and to-domain growth. Since long range diffusion is not necessary for an order-disorder phase transformation occurring in a system with a homogeneous composition,[35,36] the observation of a time square-root dependence can be surprising. However, because not all positions are equivalent in an ordered phase, atoms need in general several jumps before to contribute to the ordered configuration, leading to $k \sim 0.5$. In the third regime, a first low-energy atomic configuration has been found (well organized domains are observed), which explains the lower rate of atom ordering. A longer time will be needed in order to go from this configuration to the lowest energy one (single crystal), as the growth/consumption competition between domains of different orientation needs to explore atomic configurations of higher energy before to find a configuration promoting an energy gain to the system. This is due to the fact that an atom at the interface of two different domains needs in general several jumps before to find a site of minimum energy when leaving one domain for the other. In the case of reactive diffusion, Fig. 7 shows that the phases are not in contact when they form their first full layer. Phases nucleate locally in the concentration gradient at concentrations close to their stoichiometry. Then, the phases grow independently in their local concentration environments before coming into contact. During this first growth stage the phase volumes increase linearly with time ($k \sim 1$) in similar conditions as those for single phase formation in homogeneous stoichiometric random solid solutions. Consequently, during our reactive diffusion simulations, the first growth regime characterized by $x \propto t$ is related to the first stage of the phase formation process, in the phase local concentration environment. This linear time dependence is not related to interface effects between compounds nor to diffusion asymmetry. Once the three compound layers are in contact, their volumes cannot increase using atoms in their vicinity. The compound layers can only grow if *A* and *B* atoms diffuse through some or all of the existing layers. Thus, the compound volumes increase following a square-root time dependence, with $x \propto t^{0.5}$. We have seen that a similar regime is observed in the case of phase

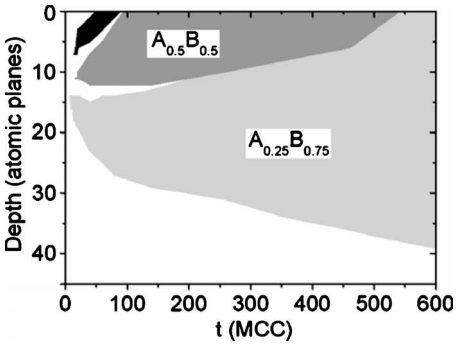

FIG. 10. Depth location of the three phases $A_{0.75}B_{0.25}$, $A_{0.5}B_{0.5}$, and $A_{0.25}B_{0.75}$, from the atomic plane 2 (subsurface plane) to the plane 44 versus time (t), in the case of the dissolution of a 10-ML-thick A layer on a B substrate.

formation in homogeneous random solutions, which corresponds to the end of domain stabilization. However, the square-root time-dependence regime during reactive diffusion is different since it results from the constant atom supply to the growing layer via atomic diffusion. This regime can exist as long as the A and B atom reservoirs are not empty.

V. SEQUENTIAL PHASE FORMATION ORIGIN

Whatever the initial thickness of the A layer deposited on the B substrate, the first stage of the dissolution consists of a rapid formation and dissolution of the $L1_0$ phase, as already presented in Fig. 5. The reactive diffusion of A and B pure layers initially separated by a 4-ML-thick $L1_0$ film also leads to the dissolution of the $L1_0$ layer and to the formation of $A_{0.25}B_{0.75}$, $A_{0.5}B_{0.5}$, and $A_{0.25}B_{0.75}$ clusters along an interfacial concentration gradient before phase formation. The phase growth time dependence is independent of the initial thickness of the film, but in the case of very thin films, a linear time dependence can only exist before dissolution.

In Figs. 10 and 11 we present the phase formation sequence in the case of the reactive diffusion of two A films with different thickness (10 ML and 5 ML, respectively) initially deposited on a B substrate. As can be seen in Fig. 10, the dissolution of the thicker 10 ML film proceeds by both simultaneous phase formation (the three phases coexist) and

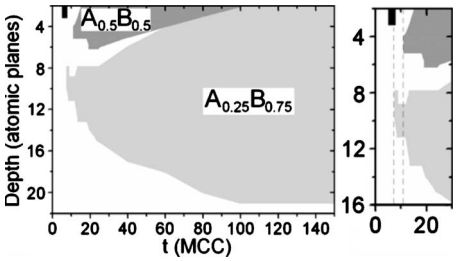

FIG. 11. Depth location of the three phases $A_{0.75}B_{0.25}$, $A_{0.5}B_{0.5}$, and $A_{0.25}B_{0.75}$, from the atomic plane 2 (subsurface plane) to the plane 24 versus time (t), in the case of the dissolution of a 5-ML-thick A layer on a B substrate. On the right side, an enlargement focused on the dissolution beginning is presented.

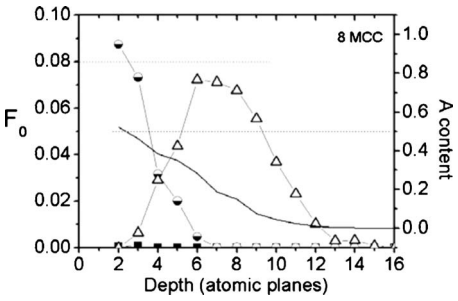

FIG. 12. Volume fraction F_0 (left axis) of the three ordered phases A-rich $L1_2$ (solid squares), $L1_0$ (semisolid circles) and B-rich $L1_2$ (open triangles), and concentration profile of A atoms (solid line, right axis) versus depth (atomic planes, bottom axis) in the case of the dissolution of a 3-ML-thick A layer on a B substrate at $t=8$ MCC.

sequential phase dissolution. Indeed, the $A_{0.75}B_{0.25}$ compound located close to the surface disappears first to the benefit of the $A_{0.5}B_{0.5}$ compound, which results in a decrease in the $A_{0.75}B_{0.25}$ thickness correlated with an increase in the $A_{0.5}B_{0.5}$ thickness. Then in a next regime, the $A_{0.5}B_{0.5}$ compound is consumed in its turn by the $A_{0.25}B_{0.75}$ compound, as can be deduced from the decrease in the thickness of the former and the increase in the latter. In the case of the thinner 5 ML deposit, it can be seen in Fig. 11 that the phase formation is sequential, the different phases appearing one after the other with the possible overlap of only two of them. The first phase to appear is $A_{0.75}B_{0.25}$, located at the surface of the sample. Then we observe the coexistence of $A_{0.75}B_{0.25}$ at the surface still, with $A_{0.25}B_{0.75}$ located deeper in the bulk. After the disappearance of $A_{0.75}B_{0.25}$, $A_{0.25}B_{0.75}$ is the only phase observed in the bulk of the sample for a little time, before the appearance of $A_{0.5}B_{0.5}$ close to the surface of the sample. Thus, $A_{0.5}B_{0.5}$ and $A_{0.25}B_{0.75}$ coexist until that $A_{0.25}B_{0.75}$ consumes $A_{0.5}B_{0.5}$ up to the surface. The appearance of $A_{0.25}B_{0.75}$ in the bulk before $A_{0.5}B_{0.5}$ close to the surface seems to be due to the consumption of $A_{0.75}B_{0.25}$ by $A_{0.5}B_{0.5}$ via a nonplanar interface (distribution of $A_{0.5}B_{0.5}$ nucleus in the region between the surface plane and the $A_{0.25}B_{0.75}$ phase). Instantaneous simulations show that 20% of the time $A_{0.5}B_{0.5}$ appears before $A_{0.25}B_{0.75}$ (but not at the same MCC), and if the initial thickness of the A layer is decreased to 4–3 ML, as shown in Fig. 12, the $A_{0.75}B_{0.25}$ phase is not observed, and $A_{0.5}B_{0.5}$ is formed at the surface of the sample before $A_{0.25}B_{0.75}$. In both cases 10 and 5 ML, all the ordered phases of the bulk phase diagram are observed. Therefore, from the comparison of Figs. 7, 10, and 11, it appears that our model is clearly able to simulate the thickness-controlled simultaneous-to-sequential phase transition. In order to understand the origin of this transition, in Fig. 13 we have plotted the depth dependence of the ordered fractions of the three phases as well as the corresponding A composition profile, at four times (3, 6, 12, and 24 MCC) characteristic of the different stages of the dissolution of the 5 ML A/B deposit determined from Fig. 11. Thus, after 3 MCC, the three phases are only found as nuclei in the composition gradient ($0<F_0<0.08$), although the concentration profile exhibits an asymmetric shape, with $0.0 \leq C_A \leq 0.9$. This asymmetry continues to in-

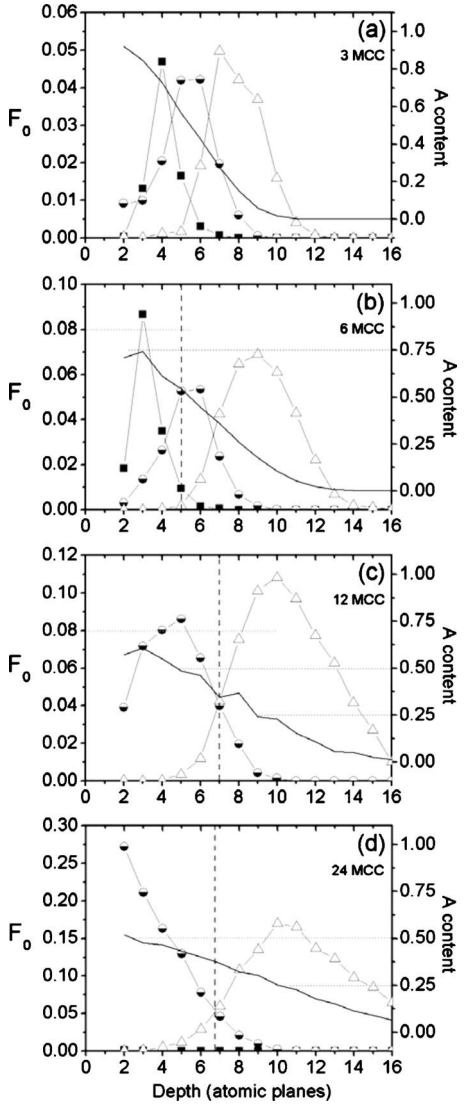

FIG. 13. Volume fraction F_0 (left axis) of the three ordered phases A-rich $L1_2$ (solid squares), $L1_0$ (semisolid triangles) and B-rich $L1_2$ (open squares), and concentration profile of A atoms (solid line, right axis) versus depth (atomic planes, bottom axis) in the case of the dissolution of a 5-ML-thick A layer on a B substrate: (a) $t=3$ MCC, (b) $t=6$ MCC, (c) $t=12$ MCC, and (d) $t=24$ MCC.

crease after 6 MCC, leading to a local concentration close to the surface $C_A \sim 0.75$ that triggers the local nucleation of the single $A_{0.75}B_{0.25}$ phase. This phase is then progressively consumed by nuclei of the $A_{0.5}B_{0.5}$ phase in a concentration gradient higher than $C_A=0.5$ while at 8 MCC $A_{0.25}B_{0.75}$ forms deeper in the bulk where $C_A \sim 0.25$. At 12 MCC the $A_{0.5}B_{0.5}$ phase forms a full layer in the gradient part where $C_A \sim 0.5$, and at 24 MCC this layer has reached the surface, as the concentration gradient in the vicinity of the surface has decreased to reach $C_A \sim 0.5$. Finally, the $A_{0.5}B_{0.5}$ layer is consumed by the $A_{0.25}B_{0.75}$ layer. These subsequent stages show that the initial phase formation process follows the same rules as for very thick layers, namely, the phases nucleate locally in the composition gradient in composition regions close to their stoichiometric compositions. The difference in their behavior with that of thick layers comes from the fact that due to the finite size of the film compared to the substrate (that can be considered as a semi-infinite medium), the interdiffusion profile formed is asymmetric, leading to sequential phase formation starting with the film-atom-rich phase. The concentration profile asymmetry can be understood by considering that, at a given time, the number of substrate atoms that enter the film is equal to the number of film atoms that enter the substrate. Due to the finite size of the film, the diffusion profile tends to form a flat gradient in the film (Fickian diffusion in finite system) but a long tail in the substrate (Fickian diffusion in semi-infinite system) of lower concentration than in the film. Consequently, an average concentration corresponding to the stoichiometry of the first film-atom-rich phase appears in the film activating the local nucleation of this phase, whereas the concentration gradient in the substrate does not offer the conditions necessary for phase nucleation. It is worth noting that this interdiffusion asymmetry appears because of size effect, even if the diffusion phenomenon is totally symmetric due to constant atomic jump frequency.

VI. COMPARISON WITH EXPERIMENTAL RESULTS

As detailed in the previous section, our KMC simulations have brought to light a linear-to-square-root growth time-dependence transition and a thickness-controlled simultaneous-to-sequential phase formation transition, in agreement with experimental observations. The linear phase growth time dependence has been attributed to the early formation stage of the phase in a local concentration environment close to its stoichiometric composition without the need for atom transport, whereas the square-root phase growth time dependence corresponds to a diffusion-controlled regime in which phase growth requires atom transport through the compound layers. On the other hand, the origin of sequential phase formation has been identified as phase formation in asymmetric interdiffusion profile. The first phase that appears during sequential formation is the richest in film atoms, in agreement with existing experiments, for example, during Si/Ni dissolution.[37] Indeed, similar to what is observed experimentally, the layer growth or consumption takes place at interfaces and all the ordered compounds of the bulk phase diagram are observed during simultaneous or sequential phase formation.

It is therefore tempting to compare in a more systematic way our simulation results with the experimental data available for the binary system Si/Ni in which the simultaneous and sequential phase formation regimes of the Ni-Si phases have been extensively studied. This is justified from the point of view of the respective bulk energies of both systems, which are somewhat similar so that no strong surface segregation effect is expected, as in our model. This is less justified due to the fact that Ni and Si do not crystallize on the same lattice, which implies that the natures of both the bonding and the crystallography vary with the respective concentrations of the two elements. However, it is still possible to analyze Si/Ni dissolution into a fixed fcc lattice, imposed by the Ni substrate, by determining an average effective V parameter from the experimental solution energies in the two

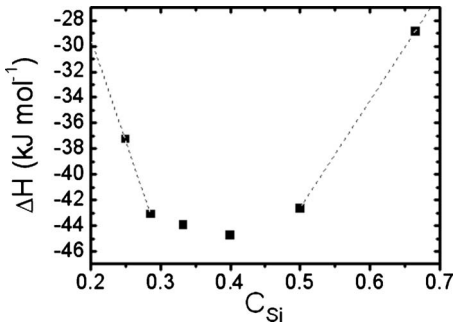

FIG. 14. Formation enthalpy (ΔH) of Ni-Si compounds versus bulk composition (C_{Si}).

dilute limits ($C \rightarrow 0$ or 1) of the $Ni_{1-c}Si_c$ compound. This is achieved by applying the usual equation relating the slope of the mixing energy E_{mix} (plotted in Fig. 14) with respect to concentration to V according to: $dE_{mix}/dC = \pm ZV$ ($\pm$ depending on $C \rightarrow 0$ or 1), where Z is the number of first neighbors (12 for the fcc structure and 4 for the diamond one). In this framework, one finds $V_{Z=12}=0.14$ eV/at and $V_{Z=4}=0.22$ eV/at, hence an average value $V=0.18$ eV/at. From this value, one can rescale the temperature axis of the bulk phase diagram in Fig. 1 by calculating the $L1_0$ order/disorder critical temperature (T_c) from the temperature dependence of the bulk long-range order parameter defined as $LRO=|C_P - C_{P+1}|$, where C_P is the layer concentration in the (001) direction, for an alternate Si/Ni perpendicular to the (001) direction. We found $T_c \sim 3673$ K, in agreement with mean-field calculus (mean-field order/disorder critical temperature $T^{MF} \sim 8276 \sim 2.25 \times T_c$) performed for the same value of V. Thus, considering the experimental Ni-Si phase formation enthalpies, one can create a pseudo Ni-Si symmetric nonregular solid solution with an fcc structure and a value of V proportional to the Ni-Si compound stability. Our KMC simulations then apply to this Ni-Si binary system for $T=10$ K.

In this context, even though our simulations are in agreement with the usual experimental observations during Si/Ni reactive diffusion,[1,7,9,11,38–40] they exhibit a few differences that should be pointed out. First, the linear-to-square-root time-dependence growth transition appears in the simulations for thicknesses significantly less than in the experiments. Indeed, we find that growth is diffusion controlled after the formation of ~1-nm-thick layers, whereas it is after a few 10-nm-thick layers from the experimental point of view. This is explained by the microstructure difference between simulations and experiments. In the simulations, the atom transport takes place on the crystal lattice and, consistent with the Metropolis algorithm, the diffusion barrier is proportional to the crystal energy difference before and after atom exchanges. Consequently, the diffusion activation energy is of same order as the phase ordering activation energy. In other words, one atomic jump from one atomic plane to another (diffusion) uses almost the same activation energy as atom ordering on a same plane (reaction). Thus, as soon as atomic transport through a few atomic planes is needed for compound layer growth, diffusion is the limiting phenomenon compared to ordering. In experiments, the growing layers are polycrystalline. Atomic diffusion uses grain boundaries (GBs), which exhibit in general diffusion coefficients that are several orders of magnitude faster than lattice diffusion coefficients. Furthermore, lower activation energies of nucleation are expected during experiments since phases usually nucleate on defects (heterogeneous nucleation). Consequently, thicker layers can grow before the diffusion kinetic becomes growth limiting, which could explain a time increase in the linear time-dependent growth regime.

As far as the simultaneous-to-sequential phase formation transition is concerned, it is found to occur for thinner deposited films in the simulations than in the experiments. For example, the simulated reactive diffusion of a 10-ML-thick film (~2 nm) exhibits simultaneous phase formation (Fig. 10), whereas the experimental reactive diffusion of a 50-nm-thick Ni film on Si leads to sequential phase formation. As previously stated, sequential phase formation appears in simulations due to phase formation in an asymmetric interdiffusion profile that results from a size effect between the film (finite medium) and the substrate (semi-infinite medium). Consistently with this mechanism, for a symmetric binary system, the lower the solubility limit of A (B) in pure B (pure A) is, the lower the critical thickness corresponding to the simultaneous-to-sequential transition should be. However, one can expect that other phenomena inducing interdiffusion asymmetry could enhance, or even prevail upon this size effect, leading to thicker critical thicknesses. This could be the case of diffusion coefficient asymmetry between the film and the substrate (at 400 °C, Ni diffusion in Si is 12 orders of magnitude faster than Si diffusion in Ni), solubility asymmetry (the solubility limit of Si in Ni is about 10% at 700 °C whereas the solubility of Ni in Si is negligible), compound stability asymmetry (the formation enthalpies of Ni-Si compounds are not symmetric around the 50% composition, Si-rich compounds are less stable, as can be seen in Fig. 14), or finally stress asymmetry (if the film and the substrate do not undergo the same stress state, diffusion and solubility are expected to be different on both sides).

Experimentally, the first phase to nucleate from dissolution of a nanometers thick Ni film into a Si substrate is in general Ni_2Si, which is richer in Ni atoms (film atoms) but not the richest (that is Ni_3Si). Furthermore, all the Ni-Si bulk phases are not observed (Ni_3Si is generally missing and $Ni_{31}Si_{12}$ as well as Ni_3Si_2 are transient phases). In our simulations, there are no missing phases and the first phase to nucleate is the film-atom richest phase. Therefore, mechanism other than diffusion-nucleation competition may play an important role in the selection of the first phase and the missing phases. Again, it is important to emphasize that an important difference between simulations and experiments is the microstructure, namely, a single crystal in simulations and a polycrystalline sample in experiments. In the latter case two types of boundaries can be defined: GBs that separate grains of a same phase and interface boundaries (IBs) that separate grains of different phases. Experimentally, the microstructure of sequentially grown phases contains both types of boundaries, GB being located in the bulk and providing atomic transport through the growing compound, whereas IBs are located at phase interfaces. Surfaces, grain boundaries, interfaces are known to exhibit different struc-

tures, atom densities, and compositions than bulk.[34,41–50] They are known also as preferential sites for lower energy heterogeneous nucleation. Grain boundaries have a thickness of 0.5 nm corresponding to 2–3 bulk atomic plane distances (transmission electron microscopy studies), and should exhibit different atom solubilities than bulk. Consequently, Boundaries could be considered as two-dimensional (2D) phases in equilibrium between 3D phases, as compared to the classical approach that only considers equilibrium between 3D phases. For example, the three phases existing in the bulk phase diagram of our binary *A*-*B* system can exist off-stoichiometry up to $\pm 10\%$. Local *A* or *B* enrichment and phase nucleation can occur at compound layer interfaces on the same fcc lattice. In contrast, as for the experimental Ni-Si system, local atom enrichment and new phase nucleation are not possible on compound lattices, since the main Ni-Si compounds are stoichiometric, and have different atomic lattices. High GB concentration gradients independent of phase solubility limit (or stoichiometry) can drive atom diffusion from one IB to another until local IB concentrations trigger phase nucleation. Thus, interdiffusion may depend on diffusion kinetic in the film and the substrate, as well as on IB equilibrium segregation driving forces.

VII. CONCLUSION

Kinetic Monte Carlo simulations have been used to simulate the reactive diffusion under dissolution of a thin *A* film deposited on a *B* substrate, in the simple case of a binary *A*-*B* system presenting a symmetrical phase diagram and no diffusion asymmetry. In agreement with experiments, these simulations lead to a linear-to-parabolic time-dependence phase growth transition and to a thickness-controlled simultaneous-to-sequential phase formation transition. The linear time-dependent growth, which corresponds to the so-called reaction-controlled growth regime, is related neither to an interface effect nor to diffusion asymmetry. Rather, it is due to the first stage of atom ordering, which is consistent with the phase nucleation process. Sequential phase formation results from the creation of an asymmetric interdiffusion profile, despite symmetric diffusion kinetics, due to the finite nature of the film and the semi-infinite nature of the substrate. In the case of sequential phase formation, we suggest that in addition to nucleation and diffusion phenomena, the understanding of equilibrium between 3D phases and their 2D interface boundaries (atom solubility, segregation, cosegregation,…) could also play an important role in the understanding of the phase sequence.

ACKNOWLEDGMENTS

The authors would like to thank D. Mangelinck and K. Hoummada for interesting discussions, as well as M. Portavoce for proofreading of the article.

*Corresponding author; alain.portavoce@im2np.fr

[1] K.-N. Tu, J. W. Mayer, and L. C. Feldman, *Electronic Thin Film Science for Electrical Engineers and Materials Scientists* (Macmillan, New York, 1992), p. 302.
[2] C. Detavernier, A. S. Özcan, J. L. Jordan-Sweet, E. A. Stach, J. Tersoff, F. M. Ross, and C. Lavoie, Nature (London) **426**, 641 (2003).
[3] C. Lavoie, C. Detavernier, C. Cabral, Jr., F. M. d'Heurle, A. J. Kellock, J. Jordan-Sweet, and J. M. E. harper, Microelectron. Eng. **83**, 2042 (2006).
[4] J. W. Christian, *The Theory of Transformations in Metals and Alloys* (Pergamon, Oxford, 1965), p. 691.
[5] E. Philofsky, Solid-State Electron. **13**, 1391 (1970).
[6] S. U. Campisano, G. Foti, E. Rimini, S. S. Lau, and J. W. Mayer, Philos. Mag. **31**, 903 (1975).
[7] M. A. Nicolet and S. S. Lau, *VLSI Electronics, Microstructure Science* (Academic Press, New York, 1983), Vol. 6, p. 330.
[8] U. Gösele and K. N. Tu, J. Appl. Phys. **53**, 3252 (1982).
[9] F. M. d'Heurle and P. Gas, J. Mater. Res. **1**, 205 (1986).
[10] S.-L. Zhang and F. M. d'Heurle, Mater. Sci. Forum **155-156**, 59 (1994).
[11] F. Nemouchi, D. Mangelinck, C. Bergman, and P. Gas, Appl. Phys. Lett. **86**, 041903 (2005).
[12] Z. Erdélyi, G. L. Katona, and D. L. Beke, Phys. Rev. B **69**, 113407 (2004).
[13] G. L. Katona, Z. Erdélyi, D. L. Beke, C. Dietrich, F. Weigl, H. G. Boyen, B. Koslowski, and P. Ziemann, Phys. Rev. B **71**, 115432 (2005).
[14] Z. Erdélyi, M. Sladecek, L.-M. Stadler, I. Zizak, G. A. Langer, M. Kis-Varga, D. L. Beke, and B. Sepiol, Science **306**, 1913 (2004).
[15] Z. Balogh, Z. Erdélyi, D. L. Beke, G. A. Langer, A. Csik, H.-G. Boyen, U. Wiedwald, P. Ziemann, A. Portavoce, and C. Girardeaux, Appl. Phys. Lett. **92**, 143104 (2008).
[16] F. M. d'Heurle, J. Mater. Res. **3**, 167 (1988).
[17] W. A. Johnson and R. F. Mehl, Trans. AIME **135**, 416 (1939).
[18] M. Avrami, J. Chem. Phys. **9**, 177 (1941).
[19] G. L. Olson and J. A. Roth, Mater. Sci. Rep. **3**, 1 (1988).
[20] D. L. Beke and Z. Erdélyi, Phys. Rev. B **73**, 035426 (2006).
[21] C. Cserháti, Z. Balogh, A. Csik, G. A. Langer, Z. Erdélyi, G. Glodán, G. L. Katona, D. L. Beke, I. Zizak, N. Darowski, E. Dudzik, and R. Feyerherm, J. Appl. Phys. **104**, 024311 (2008).
[22] C. Lavoie, F. M. d'Heurle, C. Detavernier, and C. Cabral, Microelectron. Eng. **70**, 144 (2003).
[23] G. V. Kidson, J. Nucl. Mater. **3**, 21 (1961).
[24] A. Senhaji, G. Tréglia, B. Legrand, N. T. Barrett, C. Guillot, and B. Villette, Surf. Sci. **274**, 297 (1992).
[25] A. Senhaji, G. Tréglia, J. Eugène, A. Khoutami, and B. Legrand, Surf. Sci. **287-288**, 371 (1993).
[26] G. Tréglia, B. Legrand, and F. Ducastelle, Europhys. Lett. **7**, 575 (1988).
[27] F. Ducastelle, *Order and Phase Stability in Alloys—Cohesion and Structure* (North-Holland/Elsevier Science, Amsterdam, 1991), Vol. 3.
[28] N. Metropolis, A. W. Metropolis, M. N. Rosenbluth, A. H. Teller, and E. Teller, J. Chem. Phys. **21**, 1087 (1953).

[29] J. M. Roussel, A. Saúl, G. Tréglia, and B. Legrand, Phys. Rev. B **55**, 10931 (1997).
[30] J. M. Roussel, A. Saúl, G. Tréglia, and B. Legrand, Phys. Rev. B **60**, 13890 (1999).
[31] J. M. Roussel, A. Saúl, G. Tréglia, and B. Legrand, Phys. Rev. B **69**, 115406 (2004).
[32] J. R. Manning, *Diffusion Kinetics for Atoms in Crystals* (D. Van Nostrand, Princeton, New Jersey, 1968).
[33] J. Philibert, *Atom Movements: Diffusion and Mass Transport in Solids* (Editions de Physique, Paris, 1991).
[34] H. Mehrer, *Diffusion in Solids* (Springer-Verlag, Berlin, 2007).
[35] J. D. Gunton, M. San Miguel, and P. S. Sahni, in *Phase Transitions and Critical Phenomena*, edited by C. Domb and J. L. Lebowitz (Academic, New York, 1983), Vol. 8.
[36] A. J. Bray, Adv. Phys. **43**, 357 (1994).
[37] A. Portavoce, B. Lalmi, G. Tréglia, C. Girardeaux, D. Mangelinck, B. Aufray, and J. Bernardini, Appl. Phys. Lett. **95**, 023111 (2009).
[38] P. Gas, C. Zaring, B. G. Svensson, M. Östling, C. S. Petersson, and F. M. d'Heurle, J. Appl. Phys. **67**, 2390 (1990).
[39] P. Knauth, A. Charaï, C. Bergman, and P. Gas, J. Appl. Phys. **76**, 5195 (1994).
[40] C. Lavoie, C. Coia, F. M. D'heurle, C. Detavernier, C. Cabral, P. Desjardins, and A. J. Kellock, in *Diffusion in Materials (DIMAT 2004): Proceedings of the 6th International Conference on Diffusion in Materials, Cracow, 2004*, edited by M. Danielewski, R. Filipek, R. Kozubski, W. Kucza, P. Zieba, and Z. Zurek (Scitec Publications, Switzerland, 2005), p. 825–836
[41] I. Meunier, G. Tréglia, J.-M. Gay, B. Aufray, and B. Legrand, Phys. Rev. B **59**, 10910 (1999).
[42] G. Prévot, Y. Girard, V. Repain, S. Rousset, A. Coati, Y. Garreau, J. Paul, N. Mammen, and S. Narasimhan, Phys. Rev. B **81**, 075415 (2010).
[43] M. S. Altman and E. Bauer, Surf. Sci. **344**, 51 (1995).
[44] A. Ohtake, Surf. Sci. Rep. **63**, 295 (2008).
[45] S. Olivier, A. Saúl, and G. Tréglia, Appl. Surf. Sci. **212-213**, 866 (2003).
[46] B. Legrand, G. Tréglia, and F. Ducastelle, Phys. Rev. B **41**, 4422 (1990).
[47] C. Mottet, G. Tréglia, and B. Legrand, Phys. Rev. B **46**, 16018 (1992).
[48] J. Creuze, I. Braems, F. Berthier, C. Mottet, G. Tréglia, and B. Legrand, Phys. Rev. B **78**, 075413 (2008).
[49] J. Dalmas, H. Oughaddou, C. Léandri, J.-M. Gay, G. Le Gay, G. Tréglia, B. Aufray, O. Bunk, and R. L. Johnson, Phys. Rev. B **72**, 155424 (2005).
[50] D. Wolf and S. Yip, *Materials Interfaces—Atomic-level Structure and Properties* (Chapman and Hall, London, 1992), p. 87.